Microscopic Solvation Structure of Glucose in 1-Ethyl-3-methylimidazolium Methylphosphonate Ionic Liquid

ARTICLE *in* THE JOURNAL OF PHYSICAL CHEMISTRY B · APRIL 2015

Impact Factor: 3.3 · DOI: 10.1021/acs.jpcb.5b00724 · Source: PubMed

THE JOURNAL OF PHYSICAL CHEMISTRY B

Article

pubs.acs.org/JPCB

Microscopic Solvation Structure of Glucose in 1-Ethyl-3-methylimidazolium Methylphosphonate Ionic Liquid

Kazu Hirosawa,[†] Kenta Fujii,*[,‡] Kei Hashimoto,[†] Yasuhiro Umebayashi,[§] and Mitsuhiro Shibayama*[,†]

[†]Institute for Solid State Physics, The University of Tokyo, 5-1-5 Kashiwanoha, Kashiwa, Chiba 277-8581, Japan

[‡]Graduate School of Science and Engineering, Yamaguchi University, 2-16-1 Tokiwadai, Ube, Yamaguchi 755-8611, Japan

[§]Graduate School of Science and Technology, Niigata University, 8050, Ikarashi, 2-no-cho, Nishi-ku, Niigata 950-2181, Japan

Supporting Information

ABSTRACT: The solvation structure of glucose in 1-ethyl-3-methylimidazolium methylphosphonate, $[C_2mIm^+][CH_3(H)PO_3^-]$ ionic liquid and the liquid structure of the neat $[C_2mIm^+][CH_3(H)PO_3^-]$ were investigated by high-energy X-ray diffraction (HEXRD) experiments with the aid of molecular dynamics (MD) simulations. In neat $[C_2mIm^+][CH_3(H)PO_3^-]$, a specific interaction between the cation and anion is found, that is, the oxygen atoms within $CH_3(H)PO_3^-$ are hydrogen bonded with the hydrogen of the C2 position within C_2mIm^+. In glucose/$[C_2mIm^+][CH_3(H)PO_3^-]$ solutions, a significant peak is observed at 2.6 Å in experimental radial distribution functions and is enhanced with increasing glucose concentration. It is found from MD simulations that the peak originated from the nearest-neighbor intermolecular interaction between glucose and the anion in $[C_2mIm^+][CH_3(H)PO_3^-]$. The atom−atom pair correlation function derived from MD results shows that hydroxyl groups of glucose interact with oxygen atoms within $CH_3(H)PO_3^-$ through the hydrogen bonds. The intermolecular hydrogen bonds coexist with the intramolecular hydrogen bond in a glucose molecule. We conclude that glucose is easy to form a hydrogen bond with a polar $CH_3(H)PO_3$ anion; however, rupture of intramolecular hydrogen bonds within glucose is not enough in the ionic liquid.

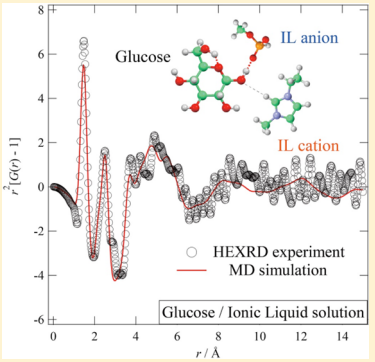

INTRODUCTION

Ionic liquids (ILs) consist of only ion species, and thus, the solvent properties of them differ from those of water or conventional organic solvents.[1] They have unique properties such as negligible volatility, nonflammability, and thermal stability and thus have been expected as novel solvents for many fields such as organic synthetic chemistry,[2,3] electrochemistry,[4−6] and soft material science.[7−10] More importantly, we can add the ability to dissolve various compounds, such as metal ions,[6,11] organic molecules,[3,12] and biopolymers,[13−15] into ILs by designing the structure of ions properly. One of the important applications of ILs is to utilize them as a solvent for cellulose, which is insoluble in water or conventional organic solvents because of their multiple intramolecular hydrogen bonds. Rogers et al. reported in 2002 that 1-butyl-3-methylimidazolim chloride, $[C_4mIm^+][Cl^-]$, dissolves cellulose under 100 °C.[16] It was the first report about ILs that dissolve cellulose, and then, many researchers made an effort to develop novel cellulose-dissolving ILs to date.[17−19] Recently, Ohno et al. reported that phosphonate-based ILs can dissolve cellulose rapidly at mild conditions, for example, 1-ethyl-3-methylimidazolium methylphosphonate, $[C_2mIm^+][CH_3(H)PO_3^-]$, dissolves 2−4 wt % cellulose at room temperature and 10 wt % at 45 °C.[18] These ILs have the ability to extract cellulose from native wood or bran and improve the energy efficiency of biomass processing of cellulose.[20] For developments of novel cellulose-dissolving ILs, solvation of cellulose in ILs plays a key role. However, knowledge at the molecular or atomistic level is still limited until now, particularly from the structural viewpoint.

To understand solute−solvent interactions in IL systems, several investigations have been reported for the IL solutions of metal ions,[21,22] organic molecules,[23−34] and polymers.[35,36] As for cellulose in IL systems, the cellulose−IL interactions, that is, the solvation structure in ILs, has been investigated using ^{13}C and $^{35/37}Cl$ NMR relaxation[37] and molecular dynamics (MD) simulations mainly.[38−41] Such previous works pointed out that the hydrogen bond networks in a cellulose crystal are ruptured by anions of ILs to form the cellulose−anion hydrogen bonds. Furthermore, it was reported by COSMO-RS calculations[42,43] and Kamlet−Taft parameters[18,44] that the solubility of cellulose can be controlled by the hydrogen bond basicity of ILs depending on the anion species. Recently, Hardacre et al. first reported the solvation structure of glucose in 1,3-dimethylimidazolium chloride, $[C_1mIm^+][Cl^-]$,[45] and 1-ethyl-3-methylimidazolium acetate, $[C_2mIm^+][CH_3COO^-]$,[46] solutions by neutron diffraction and MD simulations. They discussed the solvation structure of glucose in terms of coordination number and the space distribution of IL ions around glucose and finally concluded that the predominant interaction for cellulose dissolution is the hydrogen bond between IL anions (Cl^- or CH_3COO^-) and glucose molecules. Such experimental and

Received: January 23, 2015
Revised: March 22, 2015
Published: April 17, 2015

DOI: 10.1021/acs.jpcb.5b00724
J. Phys. Chem. B 2015, 119, 6262−6270

structural evidence of glucose−IL interactions has never been reported yet, to the best of our knowledge, except for the above study.

In this work, we chose glucose that is a monomer unit of cellulose as the model molecule to elucidate the cellulose−IL interactions. We used $[C_2mIm^+][CH_3(H)PO_3^-]$ as a solvent IL, which has the highest cellulose-dissolving ability among all of the ILs, as far as we know. We investigated the solvation structure of glucose in $[C_2mIm^+][CH_3(H)PO_3^-]$ by high-energy X-ray diffraction (HEXRD) experiments with the aid of MD simulations. First, we focused on the liquid structure, particularly the closest ion−ion interactions in neat $[C_2mIm^+][CH_3(H)PO_3^-]$, to find out the structural characteristics of $[C_2mIm^+][CH_3(H)PO_3^-]$. On the basis of this result, we extended the structural study to the solvation of glucose in $[C_2mIm^+][CH_3(H)PO_3^-]$.

EXPERIMENTAL SECTION

Materials. The IL, $[C_2mIm^+][CH_3(H)PO_3^-]$ was synthesized from 1-ethylimidazole and dimethylphosphite by reacting them in tetrahydrofuran (THF) for 2 days at 90 °C with reflux.[18] After removing THF under reduced pressure, the resulting liquid was washed with an excess amount of diethyl ether repeatedly. The residual liquid was dissolved in dichloromethane, and the resulting solution was passed through a column filled with neutral activated alumina. After removal of dichloromethane, the residual liquid was dried in vacuo at 80 °C for 48 h to give $[C_2mIm^+][CH_3(H)PO_3^-]$ as a clear and colorless liquid. Chemical identification of the obtained IL was verified using ^{1}H NMR spectroscopy and elemental analysis. The ^{1}H NMR (400 MHz, $CDCl_3$) data for $[C_2mIm^+][CH_3(H)PO_3^-]$ are as follows: δ = 1.47 (3H, t, NCH_2CH_3), 3.46 (3H, d, OCH_3), 3.96 (3H, s, NCH_3), 4.26 (2H, q, NCH_2CH_3), 6.78 (1H, d, PH), 7.38 (2H, d, NCHCHN), 10.36 (1H, s, NCHN). The results of elemental analysis are as follows: C, 41.03 (40.78); H, 6.74 (7.33); N, 13.48 (13.59), where the theoretical values calculated for $C_7H_{15}N_2O_3P$ are also shown in the parentheses. The water content in the IL prepared was checked by Karl Fischer method to be less than 500 ppm. 1-Ethylimidazole and dimethylphosphite were purchased from Wako and TCI Co., respectively, which were purified by distillation prior to use. D-Glucose was purchased from Aldrich Co. and used without further purification. Schematic illustrations for the chemical structures of $[C_2mIm^+][CH_3(H)PO_3^-]$ and D-glucose are shown in Scheme 1, together with the indices given for each atom species.

HEXRD Experiments. HEXRD measurements were carried out using the HEXRD apparatus at the BL04B2 beamline of SPring-8 (Japan Synchrotron Radiation Research Institute, JASRI, Japan).[47,48] All of the measurements were carried out under room temperature. The monochromatized X-ray of 61.6 keV was obtained using a Si(220) monochromator. The observed scattering intensity of the X-ray was corrected for absorption,[49] polarization, and incoherent scatterings[50,51] to obtain coherent scattering intensities, $I_{coh}(q)$. The experimental X-ray structure factor, $S^{exp}(q)$, and the radial distribution function, $G^{exp}(r)$, per stoichiometric volume were obtained as follows

$$S^{exp}(q) = \frac{I_{coh}(q) - \sum n_i f_i(q)^2}{\{\sum n_i f_i(q)\}^2} + 1 \quad (1)$$

$$G^{exp}(r) - 1 = \frac{1}{2\pi^2 r\rho_0}\int_0^{q_{max}} q\{S^{exp}(q) - 1\}\sin(qr) \times \exp(-Bq^2)\, dq \quad (2)$$

where n_i and $f_i(q)$ mean the number and atomic scattering factor of atom i,[52] respectively, ρ_0 is the number density, and B is the damping factor.

MD Simulations. An MD simulation for an *NTP* ensemble (298 K and 1 atm) in a cubic cell was carried out using Materials Explorer 4.0 program (Fujitsu), and the composition (number of ion pairs and D-glucose) in a given system is listed in Table S1 (Supporting Information). It is well-known that D-glucose involves some structural isomers in aqueous solution.[53−56] However, the population in $[C_2mIm^+][CH_3(H)PO_3^-]$ has never been reported yet. Hence, in this work, we used β-D-glucopyranose shown in Scheme 1 as an initial structure of the glucose molecule in the MD simulations. The simulation time was 2.0 ns for all of the systems examined here. The system was equilibrated for the first 0.5 ns with an interval of 0.2 fs, and the data collected at every 0.1 ps during 1.5−2.0 ns were analyzed to obtain the X-ray weighted structure factors and radial distribution functions, $S^{MD}(q)$ and $G^{MD}(r)$, respectively. CLaP and OPLS-AA force fields were used for IL ions and glucose, respectively,[57−61] including intermolecular Lennard-Jones and Coulombic interactions and intramolecular interactions with bond stretching, angle bending, and torsion of dihedral angles. The detailed procedure of MD simulations was described elsewhere.[36,62−70] Density values obtained by the MD simulations showed good agreement with the corresponding experimental ones, which are also listed in Table S1 (Supporting Information).

The $S^{MD}(q)$ and $G^{MD}(r)$ were calculated from the trajectory obtained by MD simulations to directly compare the MD result with HEXRD experiments, as follows

$$S^{MD}(q) = \begin{cases} \dfrac{\sum_i \sum_j \{n_i(n_j - 1)f_i(q)f_j(q)/N(N-1)\}}{\{\sum_k (n_k f_k(q)/N)\}^2} \displaystyle\int_0^r 4\pi r^2\rho_0(g_{ij}^{MD}(r) - 1)\frac{\sin qr}{qr}\, dr + 1 & (i = j) \\ \dfrac{\sum_i \sum_j \{2n_i n_j f_i(q)f_j(q)/N^2\}}{\{\sum_k (n_k f_k(q)/N)\}^2} \displaystyle\int_0^r 4\pi r^2\rho_0(g_{ij}^{MD}(r) - 1)\frac{\sin qr}{qr}\, dr + 1 & (i \neq j) \end{cases} \quad (3)$$

where the total number of atoms in the simulation box, N is given by $N = \sum_k n_k$. The X-ray radial distribution function $G^{MD}(r)$ was obtained from $S^{MD}(q)$ by a Fourier transform procedure similar to that of $G^{exp}(r)$.

RESULTS AND DISCUSSION

HEXRD Experiment. Figure 1a shows the observed $S^{exp}(q)$'s for 0−30 wt % glucose in $[C_2mIm^+][CH_3(H)PO_3^-]$ solutions in the q range of 0.2−6.0 Å^{-1}. The $S^{exp}(q)$'s at the

DOI: 10.1021/acs.jpcb.5b00724
J. Phys. Chem. B 2015, 119, 6262−6270

Scheme 1. Schematic Illustration for the Chemical Structure of $[C_2mIm^+][CH_3(H)PO_3^-]$ and Glucose, Together with the Indices Given for Each Atom Species

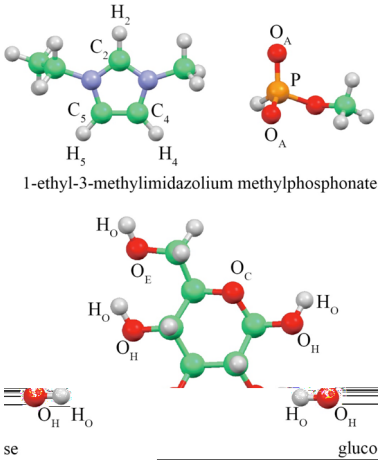

whole q range examined here (~22 Å^{-1}) are shown in Figure S1a (Supporting Information). The first peak at 1.55 Å^{-1} decreased in the intensity, and the valley at 2.5 Å^{-1} shallowed with increasing glucose concentration. Figure 1b shows the experimental radial distribution function, $G^{exp}(r)$, as a form of $r^2[G(r) - 1]$ for 0–30 wt % glucose in $[C_2mIm^+][CH_3(H)PO_3^-]$ solutions in the r range of 0–10 Å. The $G^{exp}(r)$s' in the whole r range (0–25 Å) are shown in Figure S1b (Supporting Information). In the $r^2[G^{exp}(r) - 1]$, the peaks at 2.5 and 3.0 Å appreciably increased with increasing glucose concentration. According to our previous work,[22,62,65,67,70] the intermolecular components in $G(r)$'s observed for ILs are seriously overlapped with the intramolecular ones in the r range of 3–6 Å. To elucidate the intermolecular interactions in the glucose/$[C_2mIm^+][CH_3(H)PO_3^-]$ solutions, we examined extraction of the intermolecular correlation, $G_{inter}(r)$, by subtracting the intramolecular one, $G_{intra}(r)$, from the total, $G(r)$. We thus performed MD simulations for neat $[C_2mIm^+][CH_3(H)PO_3^-]$ and glucose in $[C_2mIm^+][CH_3(H)PO_3^-]$ to obtain $G_{inter}(r)$, $G_{intra}(r)$, and total $G(r)$, which is shown in the next section.

MD Simulations. Figure 2 shows X-ray weighted radial distribution functions, $r^2[G^{MD}(r) - 1]$'s, for (a) 0 (neat IL), (b) 10, (c) 20, and (d) 30 wt % glucose in $[C_2mIm^+][CH_3(H)PO_3^-]$ solutions, together with the corresponding $r^2[G^{exp}(r) - 1]$'s

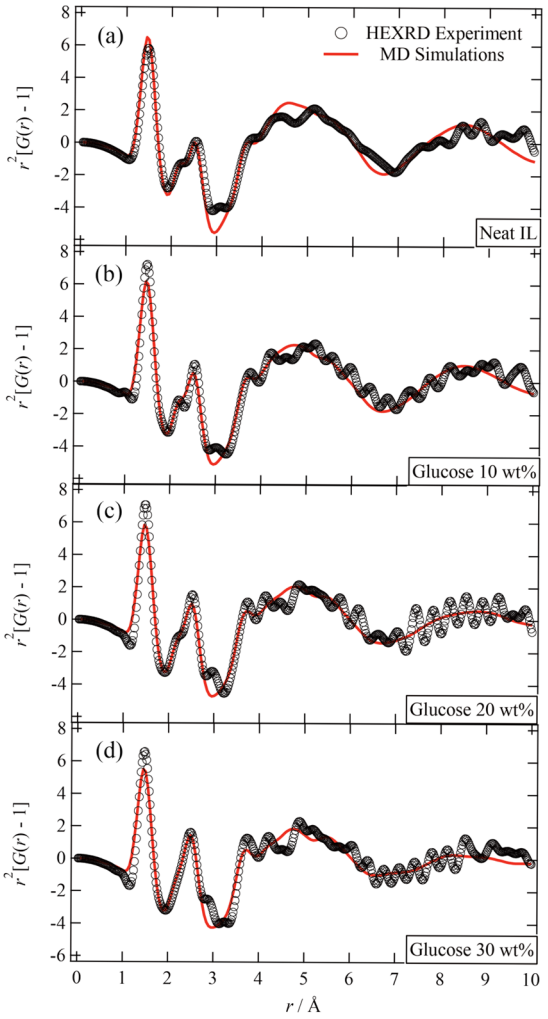

Figure 2. Radial distribution function $r^2[G(r) - 1]$ for (a) 0 (neat IL), (b) 10, (c) 20, and (d) 30 wt % glucose in $[C_2mIm^+][CH_3(H)PO_3^-]$ solutions. The open circles correspond to the experimental $r^2[G^{exp}(r) - 1]$, and the solid line with red corresponds to the theoretical $r^2[G^{MD}(r) - 1]$ derived from MD simulations.

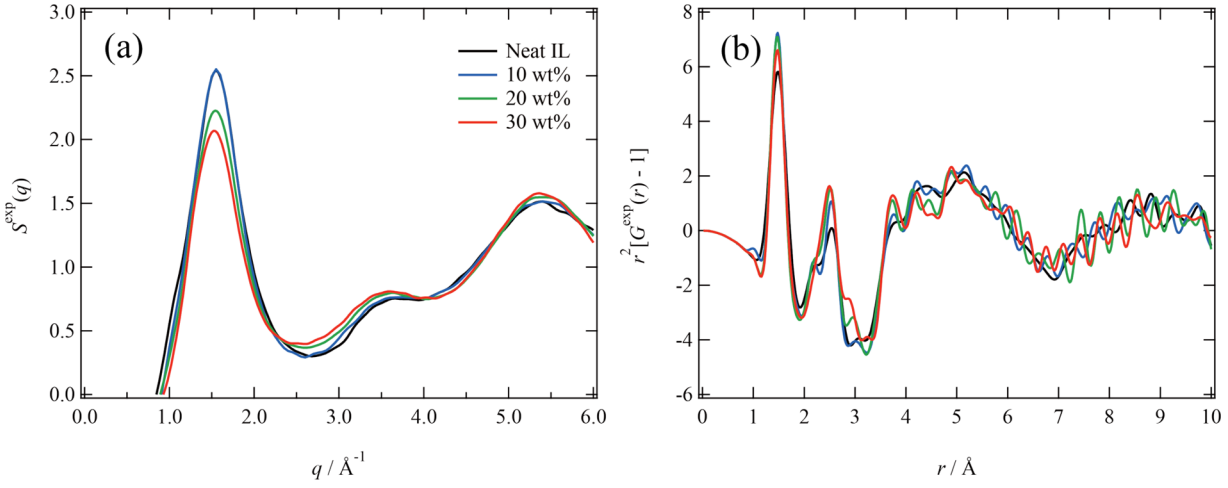

Figure 1. Glucose concentration dependence of (a) X-ray structure factors, $S^{exp}(q)$'s, and (b) radial distribution functions, $r^2[G^{exp}(r) - 1]$'s, for 0–30 wt % glucose in $[C_2mIm^+][CH_3(H)PO_3^-]$ solutions.

DOI: 10.1021/acs.jpcb.5b00724
J. Phys. Chem. B 2015, 119, 6262–6270

obtained by HEXRD experiments. It was clearly found that the MD results well reproduce the HEXRD ones for all of the glucose concentrations examined here, except for a slight disagreement between $G^{exp}(r)$ and $G^{MD}(r)$ at around 3.0 Å. The disagreement may be ascribed to the tautomerism of the glucose molecule. It is well-known that glucose coexists as two major tautomers, that is, α- and β-D-glucoses (glucopyranoses) in aqueous solutions. However, as mentioned in Experimental Section, the present MD simulations were carried out on the β-D-glucose/$[C_2mIm^+][CH_3(H)PO_3^-]$ system, not the α-D-glucose/$[C_2mIm^+][CH_3(H)PO_3^-]$ one. This is because structural information about the tautomerism of glucose in the IL system has never been reported yet. Thus, the $G^{MD}(r)$'s obtained here involve only the intramolecular component of β-D-glucose at 2.5−3.0 Å, resulting in the disagreement between $G^{exp}(r)$'s and $G^{MD}(r)$'s at around 3.0 Å. However, in this work, we mainly focused on the intermolecular interactions between glucose and $[C_2mIm^+][CH_3(H)PO_3^-]$. We assumed that the intermolecular glucose−IL interactions are essentially independent of the tautomerism of α- and β-D-glucose that have almost similar molecular structure, and then, further analysis of MD results was performed. The MD-derived total $G^{MD}(r)$ can be divided into intra- and intermolecular components, $G^{MD}_{intra}(r)$ and $G^{MD}_{inter}(r)$. We thus extracted the partial $G^{MD}_{intra}(r)$'s and $G^{MD}_{inter}(r)$'s to discuss the liquid structure of neat $[C_2mIm^+][CH_3(H)PO_3^-]$ and the solvation structure of glucose in $[C_2mIm^+][CH_3(H)PO_3^-]$. The peaks at 1.5, 2.5, and 3.0 Å in the $r^2[G(r) - 1]$ were mainly assigned to the intramolecular correlations within glucose, C_2mIm^+, and $CH_3(H)PO_3^-$ components, which are shown in Figure S2 (Supporting Information). The $G^{MD}_{inter}(r)$ is composed of six intermolecular interactions, that is, glucose−anion, glucose−cation, glucose−glucose, cation−anion, anion−anion, and cation−cation components, which are discussed in detail in the following sections.

Liquid Structure of Neat $[C_2mIm^+][CH_3(H)PO_3^-]$. $CH_3(H)PO_3^-$-based ILs show high hydrogen bond acceptor ability, which is one of the important properties to dissolve cellulose in ILs.[18] $CH_3(H)PO_3^-$ is a polar anion and therefore gives a specific liquid structure in its IL compared with well-known ILs with a bulky anion such as PF_6^-,[71] bis(fluorosulfonyl)-amide (FSA^-),[70] and bis(trifluoromethanesulfonyl)amide ($TFSA^-$).[63] We thus discussed the liquid structure of neat $[C_2mIm^+][CH_3(H)PO_3^-]$ to find out structural characteristics in the liquid state. Figure 3 shows total $G^{MD}_{inter}(r)$ as a form of $r^2[G(r) - 1]$ and the corresponding partial $G^{MD}_{inter}(r)$'s for cation−anion, anion−anion, and cation−cation components ($r^2[G^{MD}_{cat-an}(r) - 1]$, $r^2[G^{MD}_{an-an}(r) - 1]$, and $r^2[G^{MD}_{cat-cat}(r) - 1]$, respectively). Here, the partial radial distribution functions, $r^2[G^{MD}_{i-j}(r) - 1]$'s (i and j correspond to cation or anion species, respectively), are normalized by the number of combinations of ion pairs at r_{max} (=20 Å in this work) and their X-ray scattering abilities, that is, $r^2[\{G^{MD}_{i-j}(r) - G^{MD}_{i-j}(r_{max})\}/G^{MD}_{i-j}(r_{max})]$. The total $r^2[G^{MD}_{inter}(r) - 1]$ exhibited the main peaks at around 4.6, 8.5, and 12.0 Å. It is clear in partial $G^{MD}_{inter}(r)$'s that the 4.6 and 12.0 Å peaks are mainly assigned to cation−anion correlation, and the 8.5 Å one is assigned to both anion−anion and cation−cation correlations, respectively. In the $r^2[G^{MD}_{cat-an}(r) - 1]$, the peak at 4.6 Å corresponds to the distance of the closest cation−anion interaction. Here, we note that a significant peak is seen at around $r \approx 4$ Å in $r^2[G^{MD}_{cat-cat}(r) - 1]$. It was reported that a similar peak or shoulder is also found in the imidazolium-based ILs with

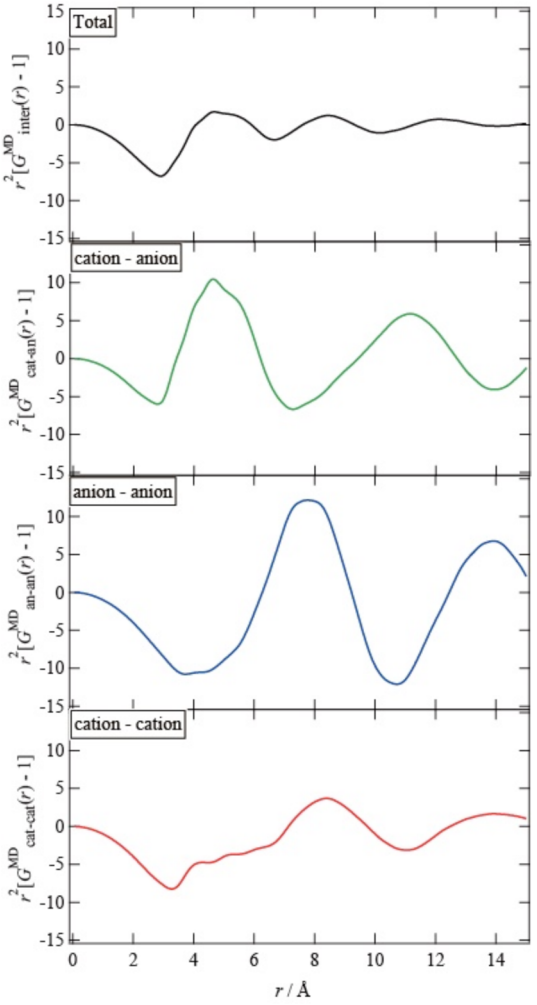

Figure 3. X-ray weighted total $G^{MD}_{inter}(r)$ as a form of $r^2[G(r) - 1]$ obtained from MD simulations for neat $[C_2mIm^+][CH_3(H)PO_3^-]$, together with partial radial distribution functions for cation−anion ($r^2[G^{MD}_{cat-an}(r) - 1]$), anion−anion ($r^2[G^{MD}_{an-an}(r) - 1]$), and cation−cation ($r^2[G^{MD}_{cat-cat}(r) - 1]$) interactions.

relatively small or polar anions such as $[C_1mIm^+][Cl^-]$[72] and $[C_2mIm^+][CH_3COO^-]$,[73] which originated from a ring-stacking between imidazolium cations. In contrast, it is not in the ILs with bulky anions such as $[C_2mIm^+][TFSA^-]$[63] and $[C_2mIm^+][FSA^-]$.[70] Therefore, we can point out that the high polarity of the $CH_3(H)PO_3^-$ anion affects not only the closest cation−anion ordering but also packing of C_2mIm^+ cations in $[C_2mIm^+][CH_3(H)PO_3^-]$.

Figure 4a and b shows spatial distribution functions (SDFs) for the center of mass of the $CH_3(H)PO_3^-$ anion around the C_2mIm^+ cation calculated from the MD trajectory. The clouds in the SDFs indicate the isoprobability surfaces of a given ion. It was found that the center of mass of the $CH_3(H)PO_3^-$ anion is located around the H_2, H_4, and H_5 (see Scheme 1) within the C_2mIm^+ cation. Here, we note the SDFs reported for typical imidazolium-based ILs, $[C_nmIm^+][X^-]$ with X = Cl^-,[72] CH_3COO^-,[73] $TFSA^-$,[63] and FSA^-,[70] n = 1, 2, or 4. The anions with high polarity (Cl^- and CH_3COO^-) tend to locate along the C_2-H_2 bond to form a hydrogen-bonding interaction between the cation and anion. On the other hand, it is quite different for the anions with low polarity and highly delocalized charge ($TFSA^-$ and FSA^-). Such anions locate above and

DOI: 10.1021/acs.jpcb.5b00724
J. Phys. Chem. B 2015, 119, 6262−6270

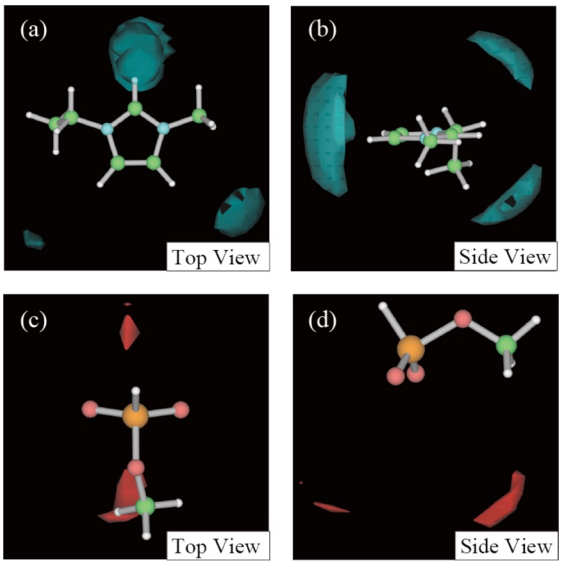

Figure 4. SDFs of the center of mass of (a,b) the $CH_3(H)PO_3^-$ anion around the C_2mIm^+ cation and (c,d) the C_2mIm^+ cation around the $CH_3(H)PO_3^-$ anion. The green and red clouds indicate the isoprobability surfaces of a given ion.

below the imidazolium ring to give no hydrogen bond between the cation and anion, and the interaction is almost from an electrostatic contribution. In this work, the $CH_3(H)PO_3^-$ anions distribute along the C_2-H_2, C_4-H_4, and C_5-H_5 bonds within the C_2mIm^+ cation, like $[C_1mIm^+][Cl^-]$ and $[C_2mIm^+][CH_3COO^-]$ systems. We concluded that the $CH_3(H)PO_3^-$ anion has high polarity and then can form a hydrogen bond with the C_2mIm^+ cation. Figure 4c and d shows SDFs for the center of mass of the C_2mIm^+ cation around the $CH_3(H)PO_3^-$ anion. It was found that the C_2mIm^+ cations distribute around two O_A atoms within the $CH_3(H)PO_3^-$ anion, and thus, the O_A atoms act as a hydrogen bond acceptor for the cation−anion interaction.

Solvation Structure of Glucose in $[C_2mIm^+][CH_3(H)PO_3^-]$. Figure 5a shows total $r^2[G^{MD}_{inter}(r) - 1]$'s for 0−30 wt % glucose in $[C_2mIm^+][CH_3(H)PO_3^-]$ solutions. The corresponding partial $r^2[G^{MD}_{inter}(r) - 1]$'s for glucose−anion and glucose−cation interactions ($r^2[G^{MD}_{glu-an}(r) - 1]$ and $r^2[G^{MD}_{glu-cat}(r) - 1]$, respectively) are shown in Figure 5b and c, respectively, which are normalized in a similar way as described above. The other components for cation−anion, cation−cation, anion−anion, and glucose−glucose interactions are shown in Figure S3 (Supporting Information). The total $r^2[G^{MD}_{inter}(r) - 1]$ exhibited a clear peak at 2.6 Å, which corresponds to the nearest-neighbor interaction in this system. It is clear from Figure 5b that the peak at 2.6 Å in the total $r^2[G^{MD}_{inter}(r) - 1]$ can be assigned to the glucose−anion interactions. The peaks at 4.0, 4.8, and 5.5 Å in the total $r^2[G^{MD}_{inter}(r) - 1]$ decreased with the glucose concentration, which mainly originated from the cation−anion interactions in the bulk according to Figure 3. The decrease in the peak intensity implies that cation−anion interactions in the bulk are ruptured to give the glucose−anion interactions. As can be seen from Figure 5c, $r^2[G^{MD}_{glu-cat}(r) - 1]$ showed a shoulder at 3.5 Å that originated from glucose−cation interactions, indicating that the C_2mIm^+ cations are the second neighbor of glucose. We thus concluded that the glucose molecules are preferentially solvated by the $CH_3(H)PO_3^-$ anion in the $[C_2mIm^+][CH_3(H)PO_3^-]$ IL, and

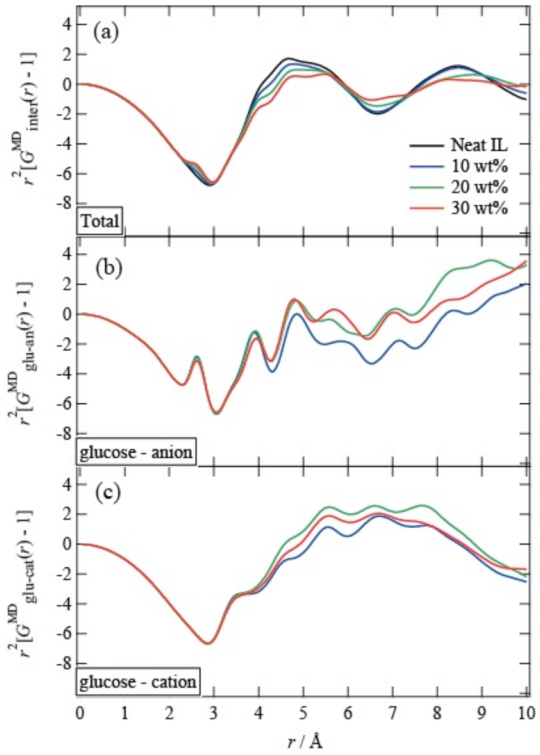

Figure 5. (a) X-ray weighted total $r^2[G^{MD}_{inter}(r) - 1]$ obtained from MD simulations for 0, 10, 20, and 30 wt % glucose in $[C_2mIm^+][CH_3(H)PO_3^-]$, together with the (b) glucose−anion ($r^2[G^{MD}_{glu-an}(r) - 1]$) and (c) glucose−cation ($r^2[G^{MD}_{glu-cat}(r) - 1]$) components.

then, contributions of the C_2mIm^+ cation to the solvation are relatively small.

Figure 6a and b shows typical SDFs calculated for O atoms (averaged both O_H and O_E components) within glucose

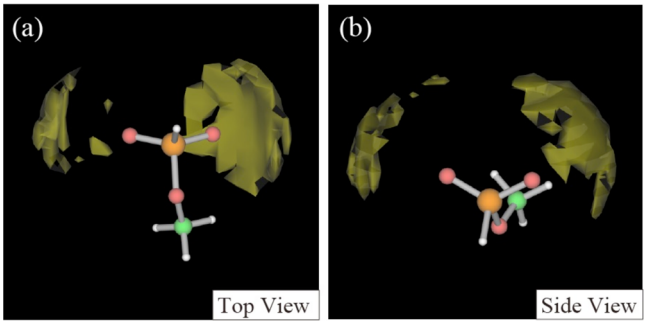

Figure 6. SDFs of O atoms (averaged for both O_E and O_H) within glucose around the $CH_3(H)PO_3^-$ anion calculated for 30 wt % glucose in the $[C_2mIm^+][CH_3(H)PO_3^-]$ system. The yellow clouds indicate the isoprobability surfaces of glucose (O atoms).

molecules around the $[CH_3(H)PO_3^-]$ anion, obtained for 30 wt % glucose in $[C_2mIm^+][CH_3(H)PO_3^-]$ solution. It was found that O atoms (glucose) locate along two $P-O_A$ bonds within the $CH_3(H)PO_3^-$ anion, and the orientation is high. The orientation indicates the existence of a hydrogen bond between O_A atoms ($CH_3(H)PO_3^-$ anion) and hydroxyl groups within glucose. On the other hand, the O atoms of the glucose molecule distribute randomly around the C_2mIm^+ cation, which is shown in Figure S4 (Supporting Information). This is because the interaction between the C_2mIm^+ cation and

DOI: 10.1021/acs.jpcb.5b00724
J. Phys. Chem. B 2015, 119, 6262−6270

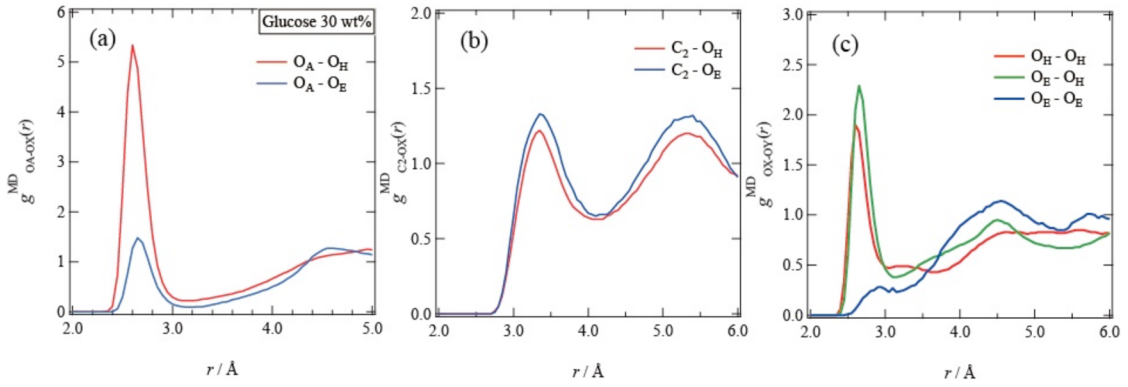

Figure 7. Atom−atom pair correlation functions, $g^{MD}_{atom-atom}(r)$, for (a) O_A (anion), (b) C_2 (cation), and (c) O_H or O_E (glucose) around O atoms within glucose calculated for 30 wt % glucose in the $[C_2mIm^+][CH_3(H)PO_3^-]$ system.

glucose originated from Coulombic force only. The SDF results are consistent with those for the partial radial distribution function discussed above, namely, glucose molecules preferentially interact with the $CH_3(H)PO_3^-$ anion relative to the C_2mIm^+ cation.

To discuss local interactions in detail, we further analyzed the present MD results to evaluate the atom−atom pair correlation functions, $g^{MD}_{atom-atom}(r)$'s. Here, we focused on the closest atom−atom interactions for intermolecular glucose−anion, glucose−cation, and glucose−glucose components. Figure 7a shows the $g^{MD}_{OA-OX}(r)$ of O_A within the $CH_3(H)PO_3^-$ anion around the O atoms (X = H or E) within glucose. The first peak in the $g^{MD}_{OA-OH}(r)$ appeared at 2.6 Å, whereas the corresponding one in the $g^{MD}_{OA-OE}(r)$ was longer than it was at 2.7 Å. The closest O (anion)···O (glucose) correlations at around 2.6−2.7 Å mainly contribute to the first peak in the total $r^2[G^{MD}_{inter}(r) - 1]$ shown in Figure 5a. Here, note that a significant difference is found in the first peak intensity among them. The difference can be explained in terms of the intramolecular hydrogen bonds within a glucose molecule, which is discussed later in detail. Figure 7b shows the $g^{MD}_{C2-OX}(r)$ of the C_2 carbon within C_2mIm^+ around the O atoms (X = H or E) within glucose. Both $g^{MD}_{C2-OX}(r)$'s exhibited the first peak at 3.4 Å. The C (cation)···O (glucose) distance of 3.4 Å is longer than the O (anion)···O (glucose) one of 2.6−2.7 Å, indicating that the O_A (anion) interacts with the hydroxyl groups (glucose) at the first neighbor and then the C_2−H_2 (cation) with the hydroxyl groups at the second neighbors. Figure 7c shows the $g^{MD}_{OX-OY}(r)$'s (X and Y = H or E) for the intermolecular O (glucose)···O (glucose) interactions between glucose molecules. The $g^{MD}_{OH-OH}(r)$ and $g^{MD}_{OE-OH}(r)$ exhibited the first peak at 2.6 and 2.7 Å, respectively, whereas no significant peak was found in the $g^{MD}_{OE-OE}(r)$. The former originated from the hydrogen bonds between glucose molecules, which contributed to the first peak in the total $r^2[G^{MD}_{inter}(r) - 1]$ shown in Figure 5, like the closest O (anion)···O (glucose) correlations, as mentioned above. The latter is due to a strong intramolecular hydrogen bond within a glucose molecule. The result indicated that intramolecular hydrogen bonds within a glucose molecule are more stably formed than intermolecular interactions between glucose molecules.

To discuss the intramolecular hydrogen bond of glucose in detail, we calculated the distribution of the dihedral angle O_C−C−C−O_E, ϕ, for the glucose molecules obtained from the MD simulations. It has been established that glucose coexists as three conformers with ϕ = 60 (gauche−trans, gt), 180 (trans−gauche, tg), and 300° (gauche−gauche, gg) in aqueous solutions, and their relative stability is in the order of gg > gt > tg based on ^{1}H NMR spectroscopy and MD simulations.[54,74,75] Figure 8 shows the distribution of ϕ in the glucose molecules

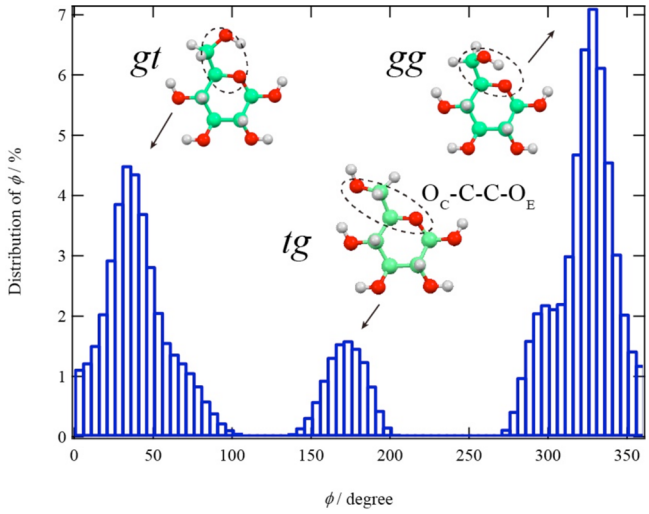

Figure 8. Histogram of the dihedral angle O_C−C−C−O_E, ϕ, of glucose molecules calculated for 30 wt % glucose in the $[C_2mIm^+]$-$[CH_3(H)PO_3^-]$ system. The interval of ϕ is 5°.

obtained by the MD simulations. Three stable glucose conformers were found in $[C_2mIm^+][CH_3(H)PO_3^-]$, like in the aqueous solution system. The distribution was largest at ϕ = 325° (gg), followed by 35 (gt) and 170° (tg). The distribution ratio of the three conformers was estimated to be gg/gt/tg = 51:38:11. The H_O−O_E of the hydroxylmethylene group was located near O_C (glucose) in the two stable conformations, gt and gg, suggesting that the conformations were stabilized by the formation of the intramolecular hydrogen bond, O_C···H_O−O_E. It is expected that the intramolecular hydrogen bond inhibits the formation of the intermolecular hydrogen bond between glucose and the anion (O_A···H_O−O_E). We assume that the relatively lower peak intensity in the $g^{MD}_{OA-OE}(r)$ in Figure 7a is ascribed to this intramolecular hydrogen bond of O_C···H_O−O_E. On the other hand, with regard to the glucose−cation interaction, the O_E (glucose) can interact with the C_2−H_2 (cation) irrespective of the intramolecular hydrogen bonds in gt, gg, and tg conformers,

DOI: 10.1021/acs.jpcb.5b00724
J. Phys. Chem. B 2015, 119, 6262−6270

resulting in no difference in the peak intensity in the $g^{MD}_{C2-OX}(r)$ (X = H, E) in Figure 7b. The coordination numbers, N_X of O_A (anion), O_H (glucose), and O_E (glucose) in the first coordination shell of O_H (glucose) are listed in Table 1,

Table 1. Coordination Number of Atoms in the First Solvation Shell of O_H−H_O in Glucose

	coordination number[a]		
concentration/wt %	O_A	O_H	O_E
10	0.87	0.03	0.02
20	0.75	0.15	0.05
30	0.62	0.29	0.08

[a]Calculated by integrating the first peak in the corresponding $g^{MD}_{X-OH}(r)$ from r = 0 to 3.0 Å.

which are calculated by the integration of $g^{MD}_{X-OH}(r)$ functions (X = O_A, O_H, O_E) up to a given r. The details of calculation were described elsewhere.[21,70] The N_{OA} decreased with increasing glucose concentration, whereas N_{OH} and N_{OE} increased with glucose concentration. This indicates that the fraction of glucose−glucose interaction increased with increasing concentration, although the glucose−anion interaction is still dominant in all concentrations. Eventually, the fraction of the glucose−glucose interacion, N_{OH} + N_{OE}, was 0.37 for 30 wt % glucose in $[C_2mIm^+][CH_3(H)PO_3^-]$. Here, note that N_{OH} was larger than N_{OE} in all of the concentration systems. The difference between N_{OH} and N_{OE} can be explained by the difference in the number of each functional group, O_H−H_O and O_E−H_O within glucose. Four O_H−H_O groups and an O_E−H_O group exist within glucose, and O_H−H_O···O_H interactions are favorably formed rather than O_H−H_O···O_E, resulting in the larger value of N_{OH} than N_{OE} around the O_H atom.

CONCLUSION

The solvation structure of glucose in $[C_2mIm^+][CH_3(H)PO_3^-]$ was investigated by HEXRD experiments and MD simulations and quantitatively discussed in terms of structural parameters such as distance, orientation, and coordination number for inter- and intramolecular interactions in the solutions. The experimental radial distribution functions, $r^2[G^{exp}(r) - 1]$'s, were well reproduced by theoretical ones derived from MD simulations for all of the systems examined here. With regards to neat $[C_2mIm^+][CH_3(H)PO_3^-]$, we pointed out that the hydrogen bond between O_A (anion) and C_2−H_2 (cation) is predominant in the cation−anion interaction due to a localized negative charge within two oxygen atoms of the anion. As for glucose in $[C_2mIm^+][CH_3(H)PO_3^-]$ solutions, it was found that the glucose molecules are preferentially solvated with the $CH_3(H)PO_3^-$ anion rather than the C_2mIm^+ cation. From the atom−atom pair correlation function, $g^{MD}_{X-X}(r)$, it was clarified that the glucose molecule is hydrogen bonded with $CH_3(H)PO_3^-$ to form the O_H−H_O (glucose)···O_A (anion) interaction. However, the intramolecular hydrogen bond of O_E−H_O···O_C within glucose still remains even in solution of $[C_2mIm^+][CH_3(H)PO_3^-]$, suppressing the interaction of O_E−H_O (glucose)···O_A (anion). Eventually, we concluded that $CH_3(H)PO_3^-$ anions preferentially form hydrogen bonds with glucose, although breakage of the intramolecular hydrogen bond within glucose is incomplete in $[C_2mIm^+][CH_3(H)PO_3^-]$.

ASSOCIATED CONTENT

Supporting Information

The composition of the systems in MD simulations, $S^{exp}(q)$'s, and $r^2[G^{exp}(r) - 1]$'s for glucose/$[C_2mIm^+][CH_3(H)PO_3^-]$ solutions at the whole q and r ranges, X-ray weighted partial radial distribution functions for intramolecular ($G^{MD}_{intra}(r)$, $G^{MD}_{glu}(r)$, $G^{MD}_{cat}(r)$, and $G^{MD}_{an}(r)$) and intermolecular ($G^{MD}_{cat-an}(r)$, $G^{MD}_{cat-cat}(r)$, $G^{MD}_{an-an}(r)$, and $G^{MD}_{glu-glu}(r)$) correlations, and SDFs of O atoms within glucose around the C_2mIm^+ cation are shown in Table S1 and Figures S1, S2, S3, and S4, respectively. The Supporting Information is available free of charge on the ACS Publications website at DOI: 10.1021/acs.jpcb.5b00724.

AUTHOR INFORMATION

Corresponding Authors

*E-mail: k-fujii@yamaguchi-u.ac.jp (K.F.).
*E-mail: sibayama@issp.u-tokyo.ac.jp (M.S.).

Notes

The authors declare no competing financial interest.

ACKNOWLEDGMENTS

This work has been financially supported by Grant-in-Aids for Scientific Research from the Ministry of Education, Culture, Sports, Science and Technology (No. 24750066 to K.F., No. 25248027 to M.S.). K.H. was supported by the Japan Society for the Promotion of Science through the Program for Leading Graduate Schools (MERIT). The HEXRD experiment was performed at BL04B2 of SPring-8 with the approval of the Japan Synchrotron Radiation Research Institute (JASRI) (Proposal Numbers 2011A1434, 2012A1571, and 2012B1502).

REFERENCES

(1) Welton, T. Room-Temperature Ionic Liquids. Solvents for Synthesis and Catalysis. *Chem. Rev.* **1999**, *99*, 2071−2083.
(2) Carmichael, A. J.; Earle, M. J.; Holbrey, J. D.; McCormac, P. B.; Seddon, K. R. The Heck Reaction in Ionic Liquids: A Multiphasic Catalyst System. *Org. Lett.* **1999**, *1*, 997−1000.
(3) Chiappe, C.; Pieraccini, D. Ionic Liquids: Solvent Properties and Organic Reactivity. *J. Phys. Org. Chem.* **2005**, *18*, 275−297.
(4) Buzzeo, M. C.; Evans, R. G.; Compton, R. G. Non-Haloaluminate Room-Temperature Ionic Liquids in Electrochemistry—A Review. *ChemPhysChem* **2004**, *5*, 1106−1120.
(5) Galinski, M.; Lewandowski, A.; Stepniak, I. Ionic Liquids as Electrolytes. *Electrochim. Acta* **2006**, *51*, 5567−5580.
(6) Seki, S.; Kobayashi, Y.; Miyashiro, H.; Ohno, Y.; Usami, A.; Mita, Y.; Kihira, N.; Watanabe, M.; Terada, S. Lithium Secondary Batteries Using Modified-Imidazolium Room-Temperature Ionic Liquid. *J. Phys. Chem. B* **2006**, *110*, 10228−10230.
(7) Ueki, T.; Watanabe, M. Upper Critical Solution Temperature Behavior of Poly(*N*-isopropylacrylamide) in an Ionic Liquid and Preparation of Thermo-sensitive Nonvolatile Gels. *Chem. Lett.* **2006**, *35*, 964−965.
(8) Ueki, T.; Watanabe, M. Lower Critical Solution Temperature Behavior of Linear Polymers in Ionic Liquids and the Corresponding Volume Phase Transition of Polymer Gels. *Langmuir* **2007**, *23*, 988−990.
(9) Kato, T. From Nanostructured Liquid Crystals to Polymer-Based Electrolytes. *Angew. Chem., Int. Ed.* **2010**, *49*, 7847−7848.
(10) Fujii, K.; Asai, H.; Ueki, T.; Sakai, T.; Imaizumi, S.; Chung, U.; Watanabe, M.; Shibayama, M. High-Performance Ion Gel with Tetra-PEG Network. *Soft Matter* **2012**, *8*, 1756−1759.
(11) Dai, S.; Ju, Y. H.; Barnes, C. E. Solvent Extraction of Strontium Nitrate by a Crown Ether Using Room-Temperature Ionic Liquids. *J. Chem. Soc., Dalton Trans.* **1999**, *8*, 1201−1202.

DOI: 10.1021/acs.jpcb.5b00724
J. Phys. Chem. B 2015, 119, 6262−6270

(12) Huddleston, J. G.; Willauer, H. D.; Swatloski, R. P.; Visser, A. E.; Rogers, R. D. Room Temperature Ionic Liquids as Novel Media for 'Clean' Liquid−Liquid Extraction. *Chem. Commun.* **1998**, *16*, 1765−1766.
(13) Madeira Lau, R.; Van Rantwijk, F.; Seddon, K. R.; Sheldon, R. A. Lipase-Catalyzed Reactions in Ionic Liquids. *Org. Lett.* **2000**, *2*, 4189−4191.
(14) Rantwijk, F.; Sheldon, R. A. Biocatalysis in Ionic Liquids. *Chem. Rev.* **2007**, *107*, 2757−2785.
(15) Moniruzzaman, M.; Kamiya, N.; Nakashima, K.; Goto, M. Water-in-Ionic Liquid Microemulsions as a New Medium for Enzymatic Reactions. *Green Chem.* **2008**, *10*, 497−500.
(16) Swatloski, R. P.; Spear, S. K.; Holbrey, J. D.; Rogers, R. D. Dissolution of Cellulose with Ionic Liquids. *J. Am. Chem. Soc.* **2002**, *124*, 4974−4975.
(17) Fukaya, Y.; Sugimoto, A.; Ohno, H. Superior Solubility of Polysaccharides in Low Viscosity, Polar, and Halogen-Free 1,3-Dialkylimidazolium Formates. *Biomacromolecules* **2006**, *7*, 3295−3297.
(18) Fukaya, Y.; Hayashi, K.; Wada, M.; Ohno, H. Cellulose Dissolution with Polar Ionic Liquids under Mild Conditions: Required Factors for Anions. *Green Chem.* **2008**, *10*, 44−46.
(19) Sun, N.; Rahman, M.; Qin, Y.; Maxim, M. L.; Rodriguez, H.; Rogers, R. D. Complete Dissolution and Partial Delignification of Wood in the Ionic Liquid 1-Ethyl-3-methylimidazolium Acetate. *Green Chem.* **2009**, *11*, 646−655.
(20) Abe, M.; Fukaya, Y.; Ohno, H. Extraction of Polysaccharides from Bran with Phosphonate or Phosphinate-Derived Ionic Liquids under Short Mixing Time and Low Temperature. *Green Chem.* **2010**, *12*, 1274−1280.
(21) Fujii, K.; Hamano, H.; Doi, H.; Song, X.; Tsuzuki, S.; Hayamizu, H.; Seki, S.; Kameda, Y.; Dokko, K.; Watanabe, M.; Umebayashi, Y. Unusual Li^+ Ion Solvation Structure in Bis(fluorosulnonyl)amide Based Ionic Liquid. *J. Phys. Chem. C* **2013**, *117*, 19314−19324.
(22) Umebayashi, Y.; Hamano, H.; Seki, S.; Minofar, B.; Fujii, K.; Hayamizu, K.; Tsuzuki, S.; Kameda, Y.; Kohara, S.; Watanabe, M. Liquid Structure of and Li^+ Ion Solvation in Bis-(trifluoromethanesulfonyl)amide Based Ionic Liquids Composed of 1-Ethyl-3-methylimidazolium and *N*-Methyl-*N*-propylpyrrolidinium Cations. *J. Phys. Chem. B* **2011**, *115*, 12179−12191.
(23) Hunger, J.; Stoppa, A.; Schrödle, S.; Hefter, G.; Buchner, R. Temperature Dependence of the Dielectric Properties and Dynamics of Ionic Liquids. *ChemPhysChem* **2009**, *2009*, 723−733.
(24) Huang, M. M.; Bulut, S.; Krossing, I.; Weingärtner, H. Communication: Are Hydrodynamic Models Suited for Describing the Reorientational Dynamics of Ions in Ionic Liquids? A Case Study of Methylimidazolium Tetra(hexafluoroisopropoxy)aluminates. *J. Chem. Phys.* **2010**, *133*, 101101.
(25) Das, S. K.; Sarkar, M. Solvation and Rotational Relaxation of Coumarin 153 and 4-Aminophthalimide in a New Hydrophobic Ionic Liquid: Role of N−H···F Interaction on Solvation Dynamics. *Chem. Phys. Lett.* **2011**, *515*, 23−28.
(26) Das, S. K.; Sarkar, M. Studies on the Solvation Dynamics of Coumarin 153 in 1-Ethyl-3-methylimidazolium Alkylsulfate Ionic Liquids: Dependence on Alkyl Chain Length. *ChemPhysChem.* **2012**, *13*, 2761−2768.
(27) Khara, D. C.; Samanta, A. Fluorescence Response of Coumarin-153 in *N*-Alkyl-*N*-methylmorpholinium Ionic Liquids: Are These Media More Structured than Imidazolium Ionic Liquids? *J. Phys. Chem. B* **2012**, *116*, 13430−13438.
(28) Das, S. K.; Sarkar, M. Rotational Dynamics of Coumarin-153 and 4-Aminophthalimide in 1-Ethyl-3-methylimidazolium Alkylsulfate Ionic Liquids: Effect of Alkyl Chain Length on the Rotational Dynamics. *J. Phys. Chem. B* **2012**, *116*, 194−202.
(29) Das, S. K.; Sahu, P. K.; Sarkar, M. Diffusion−Viscosity Decoupling in Solute Rotation and Solvent Relaxation of Coumarin 153 in Ionic Liquids Containing Fluoroalkylphosphate (FAP) Anion: A Thermophysical and Photophysical Study. *J. Phys. Chem. B* **2013**, *117*, 636−647.
(30) Khara, D. C.; Kumar, J. P.; Mondal, N.; Samanta, A. Effect of the Alkyl Chain Length on the Rotational Dynamics of Nonpolar and Dipolar Solutes in a Series of *N*-Alkyl-*N*-methylmorpholinium Ionic Liquids. *J. Phys. Chem. B* **2013**, *117*, 5156−5164.
(31) Daschakraborty, S.; Biswas, R. Dielectric Relaxation in Ionic Liquids: Role of Ion−Ion and Ion−Dipole Interactions, and Effects of Heterogeneity. *J. Chem. Phys.* **2014**, *140*, 014504.
(32) Das, S. K.; Sarkar, M. Probing Solute-Solvent Interacion in 1-Ethyl-3-methylimidazolium-Based Room Temperature Ionic Liquids: A Time-Resolved Fluorescence Anisotropy Study. *J. Fluoresc.* **2014**, *24*, 455−463.
(33) Sahu, P. K.; Das, S. K.; Sarkar, M. Fluorescence Response of a Dipolar Orgainc Solute in a Dicationic Ionid Liquid (IL): Is the Behavior of Dicationic IL Different from That of Usual Monocationic IL? *Phys. Chem. Chem. Phys.* **2014**, *16*, 12918−12928.
(34) Sahu, P. K.; Das, S. K.; Sarkar, M. Toward Understanding Solute−Solvent Interaction in Room-Temperature Mono- and Dicationic Ionic Liquids: A Combined Fluorescence Spectroscopy and Mass Spectrometry Analysis. *J. Phys. Chem. B* **2014**, *118*, 1907−1915.
(35) Matsugami, M.; Fujii, K.; Ueki, T.; Kitazawa, Y.; Umebayashi, Y.; Watanabe, M.; Shibayama, M. Specific Solvation of Benzyl Methacrylate in 1-Ethyl-3-methylimidazolium Bis-(trifluoromethanesulfonyl)amide Ionic Liquid. *Anal. Sci.* **2013**, *29*, 311−314.
(36) Asai, H.; Fujii, K.; Nishi, K.; Sakai, T.; Ohara, K.; Umebayashi, Y.; Shibayama, M. Solvation Structure of Poly(ethylene glycol) in Ionic Liquids Studied by High-Energy X-ray Diffraction and Molecular Dynamics Simulations. *Macromolecules* **2013**, *46*, 2369−2375.
(37) Remsing, R. C.; Swatloski, R. P.; Rogers, R. D.; Moyna, G. Mechanism of Cellulose Dissolution in the Ionic Liquid 1-*n*-Butyl-3-methylimidazolium Chloride: A ^{13}C and $^{35/37}Cl$ NMR Relaxation Study on Model Systems. *Chem. Commun.* **2006**, *12*, 1271−1273.
(38) Liu, H.; Sale, K. L.; Holmes, B. M.; Simmons, B. A.; Singh, S. Understanding the Interactions of Cellulose with Ionic Liquids: A Molecular Dynamics Study. *J. Phys. Chem. B* **2010**, *114*, 4293−4301.
(39) Liu, H.; Cheng, G.; Kent, M.; Stavila, V.; Simmons, B. A.; Sale, K. L.; Singh, S. Simulations Reveal Conformational Changes of Methylhydroxyl Groups during Dissolution of Cellulose I_β in Ionic Liquid 1-Ethyl-3-methylimidazolium Acetate. *J. Phys. Chem. B* **2012**, *116*, 8131−8138.
(40) Rabideau, B. D.; Agarwal, A.; Ismail, A. E. Observed Mechanism for the Breakup of Small Bundles of Cellulose I_α and I_β in Ionic Liquids from Molecular Dynamics Simulations. *J. Phys. Chem. B* **2013**, *117*, 3469−3479.
(41) Rabideau, B. D.; Agarwal, A.; Ismail, A. E. The Role of the Cation in the Solvation of Cellulose by Imidazolium-Based Ionic Liquids. *J. Phys. Chem. B* **2014**, *118*, 1621−1629.
(42) Guo, Z.; Lue, B. M.; Thomasen, K.; Meyer, A. S.; Xu, X. Predictions of Flavonoid Solubility in Ionic Liquids by COSMO-RS: Experimental Verification, Structural Elucidation, and Solvation Characterization. *Green Chem.* **2007**, *9*, 1362−1373.
(43) Kahlen, J.; Masuch, K.; Leonhard, K. Modelling Cellulose Solubilities in Ionic Liquids Using COSMO-RS. *Green Chem.* **2010**, *12*, 2172−2181.
(44) Kamlet, M. J.; Abboud, J. L. M.; Abraham, M. H.; Taft, R. W. Linear Solvation Energy Relationships. 23. A Comprehensive Collection of the Solvatochromic Parameters, π^*, α, and β, and Some Methods for Simplifying the Generalized Solvatochromic Equation. *J. Org. Chem.* **1983**, *48*, 2877−2887.
(45) Youngs, T. G. A.; Hardacre, C.; Holbrey, J. D. Glucose Solvation by the Ionic Liquid 1,3-Dimethylimidazolium Chloride: A Simulation Study. *J. Phys. Chem. B* **2007**, *111*, 13765−13774.
(46) Youngs, T. G. A.; Holbrey, J. D.; Mullan, C. L.; Norman, S. E.; Lagunas, M. C.; D'Agostino, C.; Mantle, M. D.; Gladden, L. F.; Bowron, D. T.; Hardacre, C. Neutron Diffraction, NMR and Molecular Dynamics Study of Glucose Dissolved in the Ionic Liquid 1-Ethyl-3-methylimidazolium Acetate. *Chem. Sci.* **2011**, *2*, 1594−1605.

DOI: 10.1021/acs.jpcb.5b00724
J. Phys. Chem. B 2015, 119, 6262−6270

(47) Kohara, S.; Suzuya, K.; Kashihara, Y.; Matsumoto, N.; Umesaki, N.; Sakai, I. A Horizontal Two-Axis Diffractometer for High-Energy X-ray Diffraction Using Synchrotron Radiation on Bending Magnet Beamline BL04B2 at SPring-8. *Nucl. Instrum. Methods Phys. Res., Sect. A* **2001**, *467−468*, 1030−1033.
(48) Isshiki, M.; Ohishi, Y.; Goto, S.; Takeshita, K.; Oshikawa, T. High-Energy X-ray Diffraction Deamline: BL04B2 at SPring-8. *Nucl. Instrum. Methods Phys. Res., Sect. A* **2001**, *467−468*, 663−666.
(49) Sakai, S. *KEK Report*; National Laboratory for High Energy Physics: Tsukuba, Japan, 1990; Vol. *90−16*.
(50) Cromer, D. T. Compton Scattering Factors for Aspherical Free Atoms. *J. Chem. Phys.* **1969**, *50*, 4857−4859.
(51) Cromer, D. T.; Howerton, R. J. Atomic Form Factors, Incoherent Scattering Functions, and Photon Scattering Cross Sections. *J. Phys. Chem. Ref. Data* **1975**, *4*, 471−538.
(52) Maslen, E. N.; Fox, A. G.; O'Keefe, M. A. *International Tables for Crystallography*; Kluwer: Dordrecht, The Netherlands, 1999; Vol. *C*, p 572.
(53) Lee, C. Y.; Acree, T. E.; Shallenberger, R. S. Mutarotation of D-Glucose and D-Mannose in Aqueous Solution. *Carbohydr. Res.* **1969**, *9*, 356−360.
(54) Nishida, Y.; Ohrui, H.; Meguro, H. ^{1}H-NMR Studies of (6R)- and (6S)-Deuterated d-Hexoses: Assignment of the Preferred Rotamers about C5−C6 Bond of D-Glucose and D-Galactose Derivatives in Solutions. *Tetrahedron Lett.* **1984**, *25*, 1575−1578.
(55) Maple, S. R.; Allerhand, A. Detailed Tautomeric Equilibrium of Aqueous D-Glucose. Observation of Six Tautomers by Ultrahigh Resolution Carbon-13 NMR. *J. Am. Chem. Soc.* **1987**, *109*, 3168−3169.
(56) Le Barc' H, N.; Grossel, J. M.; Loosten, P.; Mathlouthi, M. Kinetic Study of the Mutarotation of D-Glucose in Concentrated Aqueous Solution by Gas−Liquid Chromatography. *Food Chem.* **2001**, *74*, 119−124.
(57) Cornell, W. D.; Cieplak, P.; Bayly, C. I.; Gould, I. R.; Merz, K. M.; Ferguson, D. M.; Spellmeyer, D. C.; Fox, T.; Caldwell, J. W.; Kollman, P. A. A Second Generation Force Field for the Simulation of Proteins, Nucleic Acids, and Organic Molecules. *J. Am. Chem. Soc.* **1995**, *117*, 5179−5197.
(58) Damm, W.; Frontera, A.; Tirado-Rives, J.; Jorgensen, W. L. OPLS All-Atom Force Field for Carbohydrates. *J. Org. Chem.* **1997**, *18*, 1955−1970.
(59) Lopes, J. N. A. C.; Pádua, A. A. H. Modeling Ionic Liquids Using a Systematic All-Atom Force Field. *J. Phys. Chem. B* **2004**, *108*, 2038−2047.
(60) Lopes, J. N. A. C.; Gomes, M. F. C.; Pádua, A. A. H. Nonpolar, Polar, and Associating Solutes in Ionic Liquids. *J. Phys. Chem. B* **2006**, *110*, 16816−16818.
(61) Murzyn, K.; Bratek, M.; Pasenkiewicz-Gierula, M. Refined OPLS All-Atom Force Field Parameters for *n*-Pentadecane, Methyl Acetate, and Dimethyl Phosphate. *J. Phys. Chem. B* **2013**, *117*, 16388−16396.
(62) Fukuda, S.; Takeuchi, M.; Fujii, K.; Kanzaki, R.; Takamuku, T.; Chiba, K.; Yamamoto, H.; Umebayashi, Y.; Ishiguro, S. Liquid Structure of *N*-Methyl-*N*-pyrrolidinium Bis-(trifluoromethanesulfonyl)amide Ionic Liquid Studied by Large Angle X-ray Scattering and Molecular Dynamics Simulations. *J. Mol. Liq.* **2008**, *143*, 2−7.
(63) Fujii, K.; Soejima, Y.; Kyoshoin, Y.; Fukuda, S.; Kanzaki, R.; Umebayashi, Y.; Yamaguchi, T.; Ishiguro, S.; Takamuku, T. Liquid Structure of Room-temperature Ionic Liquid, 1-Ethyl-3-methylimidazolium Bis-(trifluoromethanesulfonyl) Imide. *J. Phys. Chem. B* **2008**, *112*, 4329−4336.
(64) Fujii, K.; Seki, S.; Fukuda, S.; Takamuku, T.; Kohara, S.; Kameda, Y.; Umebayashi, Y.; Ishiguro, S. Liquid Structure and Conformation of a Low-Viscosity Ionic Liquid, *N*-Methyl-*N*-ropylpyrrolidinium Bis(fluorosulfonyl) Imide Studied by High-Energy X-ray Scattering. *J. Mol. Liq.* **2008**, *143*, 64−69.
(65) Umebayashi, Y.; Chung, W.-L.; Mitsugi, T.; Fukuda, S.; Takeuchi, M.; Fujii, K.; Takamuku, T.; Kanzaki, R.; Ishiguro, S. Liquid Structure and the Ion−Ion Interaction of Ethylammonium Nitrate Ionic Liquid Studied by Large Angle X-ray Scattering and Molecular Dynamics Simulations. *J. Comput. Chem. Jpn.* **2008**, *7*, 125−134.
(66) Fujii, K.; Mitsugi, T.; Takamuku, T.; Yamaguchi, T.; Umebayashi, Y.; Ishiguro, S. Effect of Methylation at the C2 Position on the Liquid Structure of Ionic Liquids Revealed by Large-Angle X-ray Scattering Experiments and MD Simulations. *Chem. Lett.* **2009**, *38*, 340−341.
(67) Kanzaki, R.; Mitsugi, T.; Fukuda, S.; Fujii, K.; Takeuchi, M.; Soejima, Y.; Takamuku, T.; Yamaguchi, T.; Umebayashi, Y.; Ishiguro, S. Ion−Ion Interaction in Room Temperature Ionic Liquid 1-Ethyl-3-methylimidazolium Tetrafluoroborate Studied by Large-Angle X-ray Scattering Experiment and Molecular Dynamics Simulations. *J. Mol. Liq.* **2009**, *147*, 77−82.
(68) Umebayashi, Y.; Hamano, H.; Tsuzuki, S.; Lopes, J. N. A. C.; Pádua, A. A. H.; Kameda, Y.; Kohara, S.; Yamaguchi, T.; Fujii, K.; Ishiguro, S. Dependence of the Conformational Isomerism in 1-*N*-Butyl-3-methylimidazolium Ionic Liquids on the Nature of the Halide Anion. *J. Phys. Chem. B* **2010**, *114*, 11715−11724.
(69) Fujii, K.; Kanzaki, R.; Takamuku, T.; Kameda, Y.; Kohara, S.; Kanakubo, M.; Shibayama, M.; Ishiguro, S.; Umebayashi, Y. Experimental Evidences for Molecular Origin of Low-Q peak in Neutron/X-ray Scattering of 1-Alkyl-3-methylimidazolium Bis-(trifluoromethanesulfonyl)amide Ionic Liquids. *J. Chem. Phys.* **2011**, *135*, 244502.
(70) Fujii, K.; Seki, S.; Ohara, K.; Kameda, Y.; Doi, H.; Saito, S.; Umebayashi, Y. High-Energy X-ray Diffraction and MD Simulation Study on the Ion−Ion Interaction in 1-Ethyl-3-methylimidazolium Bis(fluorosulfonyl)amide. *J. Solution Chem.* **2014**, *43*, 1655−1668.
(71) Hardacre, C.; McMath, S. E. J.; Nieuwenhuyzen, M.; Boeron, D. T.; Soper, A. K. Liquid Structure of 1,3-Dimethylimidazolium Salts. *J. Phys.: Condens. Matter* **2003**, *15*, S159−S166.
(72) Hardacre, C.; Holbrey, S. E. J.; McMath, S. E. J.; Boeron, D. T.; Soper, A. K. Structure of Molten 1,3-Dimethylimidazolium Chloride Using Neutron Diffraction. *J. Chem. Phys.* **2003**, *18*, 273−278.
(73) Bowron, D. T.; Agostino, C. D.; Gladden, L. F.; Hardacre, C.; Holbrey, J. D.; Lagunas, M. C.; McGregor, J.; Mantle, M. D.; Mullan, C. L.; Youngs, T. G. A. Structure and Dynamics of 1-Ethyl-3-methylimidazolium Acetate via Molecular Dynamics and Neutron Diffraction. *J. Phys. Chem. B* **2010**, *1214*, 7760−7768.
(74) Corchado, J. C.; Sánchez, M. L.; Aguilar, M. A. Theoretical Study of the Relative Stability of Rotational Conformers of α and β-D-Glucopyranose in Gas Phase and Aqueous Solution. *J. Am. Chem. Soc.* **2004**, *126*, 7311−7319.
(75) Bagno, A.; Rastrelli, F.; Saielli, G. Prediction of the ^{1}H and ^{13}C NMR Spectra of α-D-Glucose in Water by DFT Methods and MD Simulations. *J. Org. Chem.* **2007**, *72*, 7373−7381.

DOI: 10.1021/acs.jpcb.5b00724
J. Phys. Chem. B 2015, 119, 6262−6270